34th Annual International Conference of the IEEE EMBS
San Diego, California USA, 28 August - 1 September, 2012

Valvular Closure Prediction using Anisotropic and Hyperelastic Tissue models and Individualized Anatomy Derived from RT3DE

C. Sprouse[1], R. Mukherjee[1], and P. Burlina[1,2]

Abstract— **We describe a method for modeling the closure of the Mitral Valve (MV) and to compute realistic strain and stresses in MV tissues. This informs preoperative planning by allowing a surgeon to evaluate various MV repairs options. The modeling method exploits individualized (patient-specific) anatomical structure recovered from real-time 3D echocardiography (RT3DE). This study utilizes hyperelastic models of the MV tissues and employs patient specific leaflets, chordal length assessment and annulus shapes. We report experiments on ten intraoperative test cases, where we compute strain and stresses using several different tissue models from MV empirical studies by May-Newman [1] and Holzapfel [2].**

I. Introduction

Mitral valve modeling has a number of applications in diagnostics and computer assisted surgery. The mitral valve is a critical structure found in the left heart and located between the left atrium (LA) and the left ventricle (LV), ensuring unidirectional blood flow from LA to LV. It is composed of an annulus with two leaflets tethered through a system of chords (termed *chordae tendineae*) attached to papillary muscles. MV surgery (valvuloplasty) is a complex intervention with different repair options. Therefore simulation tools would be of critical help to surgeons to elucidate which valvuloplasty option is most likely to improve outcome. Our simulation-based planning process starts with an open 3D valve structure at diastole, derived by segmenting RT3DE imagery and edited by a surgeon to remove artifacts and reflect the planned surgical modifications [3], [4]. From the open valve, our system predicts, via physics-based modeling and simulation, the closed valve configuration at systole to characterize the MV leaflets' ability to competently coapt, and the associated strains and stresses for this closed configuration, when the system is under systolic pressure.

Much progress has been made in MV modeling [5]. The recent availability of real time echographic 3D data has now made possible the goal of MV simulation using patient-specific anatomy, as well as the possibility of benchmarking against ground truth datasets [4], [6], [7], [8], [9], [12], [13].

Unlike our prior work in [4], which used linear elastic constitutive models, this study uses a hyperelastic tissue models to infer resultant stresses. The contributions of this paper are: the joint use of hyperelastic models and patient specific anatomy to predict the closure state and the stresses associated with a specific valve repair. This paper extends our study in [10] in several ways: we now use patient specific annulus shapes, we estimate patient-specific chordal length factors, we extend our testing use cases from an original sample set of two to ten, and we test using several elastic energy models and parameter sets that were derived empirically by studies conducted by May-Newman in [1] and Holzapfel in [2].

[1]The Johns Hopkins University Applied Physics Laboratory, Laurel, MD 20723, and [2]The Johns Hopkins University Computer Science Department, Baltimore, MD 21218

II. Method

A mesh representing the patient-specific MV anatomy is first derived by first performing segmentation using thin tissue detection [11]. At each node of the mesh we prescribe either displacements or forces. Modeled forces include those due to fluid pressure, hyperelastic stress, collision with other portions of the mesh, and tethering of the valve to the chordae tendineae. The initial configuration of the open mesh is used to specify the reference energy point for external and internal forces. The steady state configuration of the valve system under load at a closed position, where all forces are at equilibrium, is then found by minimizing the system's total energy.

Our prior work focused on predicting the closed configuration of the mitral valve from an open configuration obtained from segmented 3D ultrasound imagery. Given this capability, it is possible to predict the closure of a modified valve by making modifications to the segmented valve model which simulate the changes to the valve structure made during a valvuloplasty procedure and assess resultant coaptation. However, besides the coaptation of the valves, other valuable information may be obtained from the current modeling approach. In particular, high leaflet stress may result in decreased longevity and hence the ability to predict the stresses induced in the leaflet may also inform valvuloplasty decisions. In the present work we focus on modeling of stresses and strains within the mitral valve leaflets.

Following our prior work [10] we use an energy minimization approach to find the closed valve configuration from an initial open configuration. The potential energy minimized is

$$\Phi = \sum_{\text{all nodes } i} \phi_i^X + \phi_i^T + \phi_i^C + \phi_i^E, \tag{1}$$

where the terms represent the external, tethering, collision, and elastic energy respectively. The tethering and collision terms remain unchanged from those previously reported in [4]. In this study, the force acting on the facets by the fluid pressure is now directed along the facet normal, and the elastic term is modified to allow for hyperelastic material behavior other than the St. Venant-Kirchhoff model.

Hyperelastic materials are a class of elastic materials for which the stress-strain relationship is derivable from a strain

978-1-4577-1787-1/12/$26.00 ©2012 IEEE

energy density function, Ψ. The hyperelastic models used in this paper are

1) St. Venant-Kirchoff (SVK)

$$\Psi_{\mathrm{S}} = \frac{1}{2}\,\mathrm{tr}\,\mathbf{SE}, \tag{2}$$

where

$$\mathbf{S} = \frac{E}{1+\nu}\left[\mathbf{E} + \frac{\nu}{1-2\nu}(\mathrm{tr}\,\mathbf{E})\mathbf{1}\right], \tag{3}$$

for Young's modulus E, and Poisson ratio ν. A more extensive treatment of this model is provided in [3].

2) May-Newman-Yin (MNY)

$$\Psi_{\mathrm{M}} = c_0\left[e^{c_1(I_1-3)^2+c_2(\lambda-1)^4} - 1\right], \tag{4}$$

where $I_1 = \mathrm{tr}\,\mathbf{C}$ is the first invariant of the right Cauchy-Green deformation tensor and $\lambda = \sqrt{\widehat{\mathbf{a}}_0\mathbf{C}\widehat{\mathbf{a}}_0}$ is the stretch in the $\widehat{\mathbf{a}}_0$ direction. The vector $\widehat{\mathbf{a}}_0$ is chosen parallel to the orientation of the collagen fiber to model the increased stiffness in the fiber direction relative to the transverse directions. The values of the coefficients c_i are taken from [1].

3) Holzapfel

$$\Psi_{\mathrm{H}} = c_0'\left[e^{c_1'(I_1-3)^2+c_2'(\lambda^2-1)^2} - 1\right], \tag{5}$$

with I_1 and λ as above, and the coefficients c_i' are taken from [2].

The leaflets are modeled as thin membranes using a plane-stress assumption.

Four canonical situations are typically reported when characterizing the stress-strain behavior: the first is for equibiaxial deformation in which the membrane is deformed in directions parallel and perpendicular to the fiber direction equally. The second is off-biaxial in which the membrane is deformed parallel and perpendicular to the fiber direction with the perpendicular deformation equal to 1.5 times the parallel deformation. The third is parallel strip-biaxial in which the membrane is deformed parallel to the fiber direction while keeping the perpendicular deformation fixed at +15%. The fourth is perpendicular strip-biaxial in which the membrane is deformed perpendicular to the fiber direction while keeping the parallel deformation fixed at +15%.

Representative stress-strain curves are shown in Figs. 1 and 2 for the three hyperelastic laws and for the various MNY specimens. The MNY law with mean parameters and the Holzapfel laws agree for strains greater than approx. 5%, while the SVK parameters were chosen to cross the equibiaxial MNY mean curve at approximately 15% and hence is much stiffer for small strains than either of the Fung-type laws. The considerable variation in stiffness among the MNY specimens is evident in both figures.

Parameters used for each of the models are shown in Tables I and II. The MNY parameters are taken from [1], and both the values obtained for individual specimens and the average parameters are modeled. The Holzapfel parameters are from [2]. The parameter values for the SVK model are chosen to match the MNY mean curve for deformation of +15%.

TABLE I

ANTERIOR LEAFLET MATERIAL PROPERTIES.

Case	c_0 (Pa)	c_1	c_2	d (mm)
CP01	1010	2.59	1376.9	0.68
CP02	79	1.25	1320.6	0.86
CP03	181	7.01	626.5	1.40
CP04	214	4.90	1602.9	0.86
CP05	105	5.23	1991.6	0.98
CP06	203	1.76	833.0	0.78
CP07	53	6.31	1943.2	0.76
CP08	2171	2.19	1408.8	0.48
MNY	399	4.325	1446.5	0.85
Holzapfel	52	4.63	22.6	0.85
SVK	$E = 400$ kPa, $\nu = 1/2$			1

TABLE II

POSTERIOR LEAFLET MATERIAL PROPERTIES.

Case	c_0 (Pa)	c_1	c_2	d (mm)
CP01	519	2.65	103.1	0.57
CP02	278	5.23	478.8	0.55
CP03	268	4.28	4.8	0.44
CP04	762	2.33	116.8	0.85
CP05	1507	2.91	1215.7	0.41
CP06	399	2.14	320.3	0.44
CP07	4176	2.16	249.2	0.52
CP08	426	6.74	81.1	0.43
MNY	414	4.848	305.4	0.53
Holzapfel	171	5.28	6.46	0.53
SVK	$E = 100$ kPa, $\nu = 1/2$			1

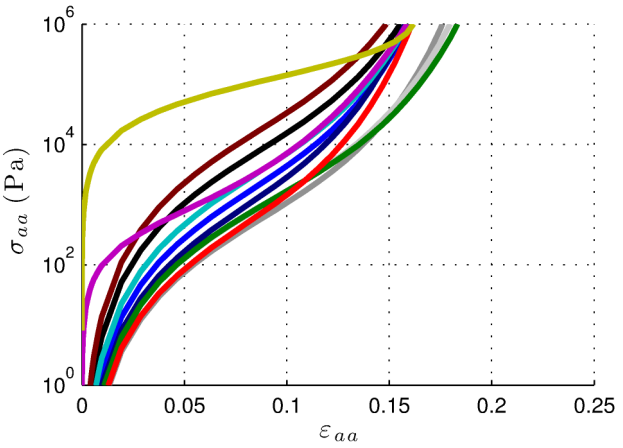

Fig. 1. Stress-strain relationship for the anterior leaflet for equibiaxial deformation varying between -50% and $+50\%$. Stress parallel to the fiber direction (σ_{aa}) is plotted versus strain parallel to the fiber direction ($\varepsilon_{\mathrm{aa}}$). Curves represent hyperelastic model with particular parameter sets, MNY specimens CP01 through CP08 (black, dark gray, light gray, blue, dark blue, green, red, and dark red respectively), MNY "mean" (cyan), Holzapfel (magenta), SVK (yellow).

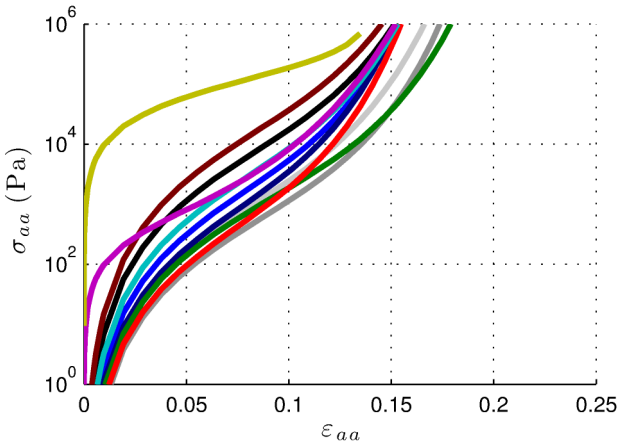

Fig. 2. Stress-strain relationship for the anterior leaflet for off-biaxial deformation with parallel deformations varying between -50% and $+50\%$. Stress parallel to the fiber direction (σ_{aa}) is plotted versus strain parallel to the fiber direction (ε_{aa}). Curves are as described in Fig. 1.

III. Experiments

We use intraoperative RT3DE transesophageal full volume sequence of the left heart. The RT3DE acquisition was performed using an iE33 Philips console with a Philips X7-2t Live probe (Philips Medical Systems, Bothell, WA). The RT3DE cube sizes were $208\times208\times224$. The RT3DE probe was operated at frequencies ranging from 3 to 5 MHz and frame rate up to 50 Hz. The pixels' spatial resolutions were respectively ranged between 0.4 to 0.8 mm. The chordal lengths and the annulus were personalized (more details on this and other methods and acquisition are provided in [3]).

Benchmarking was performed using ten RT3DE cases and was carried out by computing absolute errors between (a) the closed valve configuration predicted at systole from the segmented open valve captured at diastole, and (b) the closed valve segmented during systole. We found on average mean absolute errors ranging from 1.2 to 1.9 mm across the different models.

The RT3DE-based closed state simulations resulted in physiological strains and plausible stresses which are consistent with other modeling and empirical studies in [1], [5], [12], [13]. Fig. 3 shows the distribution for the radial strains on the predicted closed valve for one of the cases. Fig. 4 shows the distribution of the radial stress. Box plots showing median, standard deviation and extremal values for anterior and posterior stress are shown in Figs. 5(a) and 5(b). Similarly, strain is shown in Figs. 6(a) and 6(b).

The SVK model underpredicts the strain relative to the Fung-type models. This is to be expected as this model is much stiffer for small displacements than the others. The stress predicted by the SVK model is consistent with the other models.

IV. Conclusions

We report on a new RT3DE-guided physics-based modeling and simulation procedure to predict the stresses and strains for a closed state MV from an open MV configuration exploiting a shape finding optimization method. Testing with clinical data shows the ability to predict stress/strain values that are consistent with prior published modeling and empirical studies.

Acknowledgments

We would like to thank Dr. May-Newman (SDSU) for interesting discussions. This project was supported in part by JHU APL Science and Technology Research and Development funds and by NIH NHLBI R21HL098765. The content is solely the responsibility of the authors and does not necessarily represent the official views of the National Heart, Lung, and Blood Institute of the National Institutes of Health.

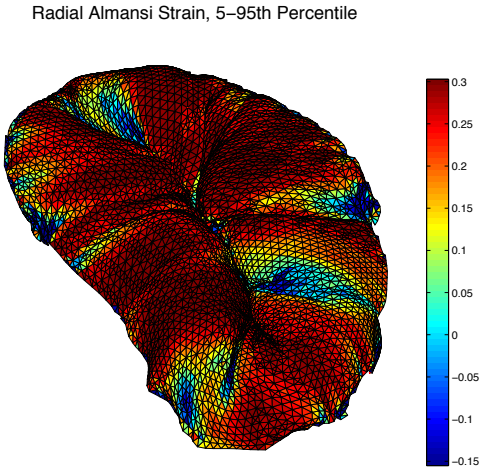

Fig. 3. Radial Almansi strain for each facet overlaid on the simulated closed-state mesh. The starting mesh consisted of approximately 21,000 facets, and the simulation was run using the average of May-Newman's hyperelastic parameters.

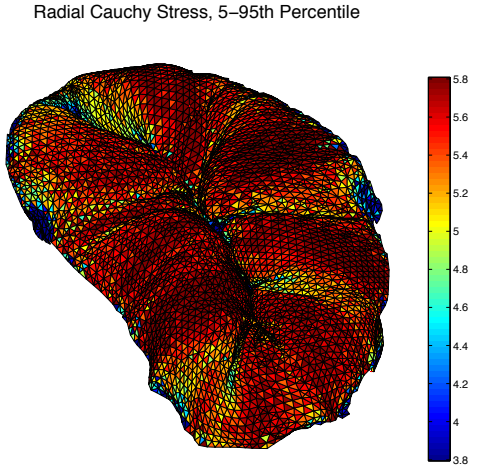

Fig. 4. Radial Cauchy stress for each facet overlaid on the simulated closed-state mesh. The starting mesh consisted of approximately 21,000 facets, and the simulation was run using the average of May-Newman's hyperelastic parameters. Note that the color-scale is in units of $\log_{10}$ Pa.

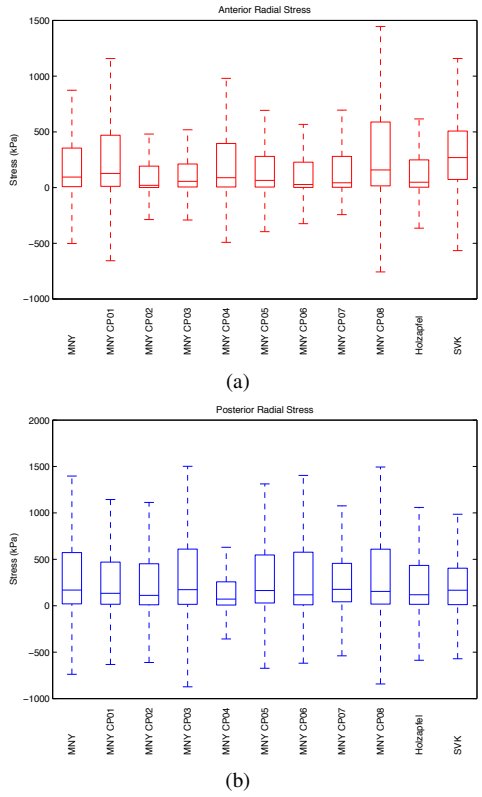

Fig. 5. Box plots depicting the radial Cauchy stress for the anterior (a) and posterior (b) leaflets across all experiments tested, as well as for each set of parameters (as specified on the x-axis).

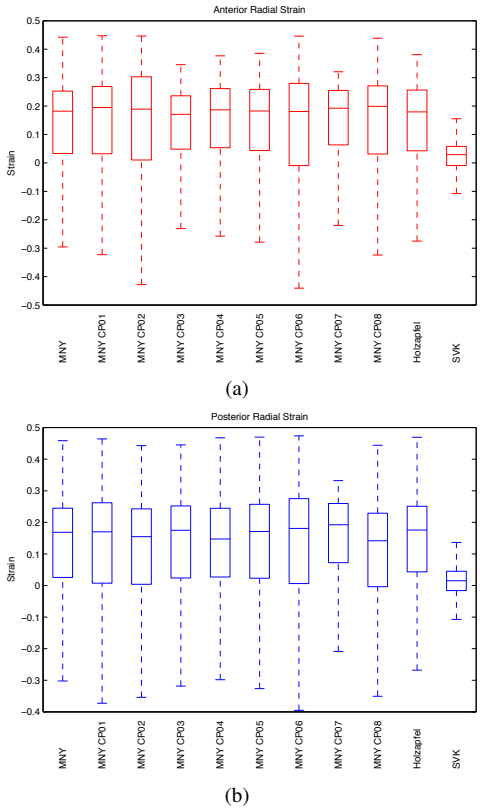

Fig. 6. Box plots depicting the radial Almansi strain for the anterior (a) and posterior (b) leaflets across all experiments tested, as well as for each set of parameters (as specified on the x-axis).

REFERENCES

[1] K. May-Newman and F. Yin, "A constitutive law for mitral valve tissue," *Journal of Biomechanical Engineering*, vol. 120, p. 38, 1998.

[2] V. Prot, B. Skallerud, and G. Holzapfel, "Transversely isotropic membrane shells with application to mitral valve mechanics. Constitutive modelling and finite element implementation," *Int. Journal for Numerical Methods in Engineering*, vol. 71, no. 8, pp. 987–1008, 2007.

[3] P. Burlina, R. Mukherjee, and C. Sprouse, "A personalized mitral valve closure simulator," in *Eng. Med. Bio. Conf.*, 2012.

[4] P. Burlina, C. Sprouse, D. DeMenthon, A. Jorstad, R. Juang, F. Contijoch, T. Abraham, D. Yuh, and E. McVeigh, "Patient-specific modeling and analysis of the mitral valve using 3D-TEE," *Information Processing in Computer-Assisted Interventions*, pp. 135–146, 2010.

[5] D. Einstein, F. Del Pin, X. Jiao, A. Kuprat, J. Carson, K. Kunzelman, R. Cochran, J. Guccione, and M. Ratcliffe, "Fluid-structure interactions of the mitral valve and left heart: Comprehensive strategies, past, present and future," *Int. Journal for Numerical Methods in Biomedical Engineering*, vol. 26, no. 3-4, pp. 348–380, 2010.

[6] C. Sprouse, D. Yuh, T. Abraham, and P. Burlina, "Computational hemodynamic modeling based on transesophageal echocardiographic imaging," *Proc. Int. Conf. Engineering in Medicine and Biology Society*, vol. 2009, pp. 3649–3652, 2009.

[7] P. E. Hammer, D. P. Perrin, P. J. del Nido, and R. D. Howe, "Image-based mass-spring model of mitral valve closure for surgical planning," in *Proc. of SPIE*, San Diego, CA, USA, 2008, pp. 69 180Q–69 180Q–8.

[8] M. Stevanella, G. Krishnamurthy, E. Votta, J. Swanson, A. Redaelli, and N. Ingels Jr, "Mitral leaflet modeling: Importance of in vivo shape and material properties," *Journal of biomechanics*, 2011.

[9] T. Mansi, I. Voigt, E. Mengue, R. Ionasec, B. Georgescu, T. Noack, J. Seeburger, and D. Comaniciu, "Towards patient-specific finite-element simulation of mitralclip procedure," *Medical Image Computing and Computer-Assisted Intervention–MICCAI 2011*, pp. 452–459, 2011.

[10] C. Sprouse, D. DeMenthon, J. Gammie, and P. Burlina, "Patient specific modeling of stress strain for surgical planning and guidance," *Proc. Int. Conf. Engineering in Medicine and Biology Society*, vol. 2011, 2011.

[11] P. Burlina, R. Mukherjee, R. Juang, and C. Sprouse, "Recovering endocardial walls from 3D TEE," *Functional Imaging and Modeling of the Heart*, pp. 284–293, 2011.

[12] E. Votta, E. Caiani, F. Veronesi, M. Soncini, F. Montevecchi, and A. Redaelli, "Mitral valve finite-element modelling from ultrasound data: a pilot study for a new approach to understand mitral function and clinical scenarios," *Philosophical Transactions of the Royal Society A: Mathematical, Physical and Engineering Sciences*, vol. 366, no. 1879, p. 3411, 2008.

[13] E. Votta, F. Maisano, S. Bolling, O. Alfieri, F. Montevecchi, and A. Redaelli, "The geoform disease-specific annuloplasty system: a finite element study," *The Annals of thoracic surgery*, vol. 84, no. 1, pp. 92–101, 2007.